Downloaded from jpg.inio.ac.ir at 8:54 IRST on Sunday December 5th 2021

Journal of the Persian Gulf
(Marine Science)/Vol. 9/No. 34/ December 2018/9/55-63

Issue of Second International Conference on Oceanography for West Asia (RCOWA) 2020

Extraction of coastlines from satellite images using sub-pixel algorithms

Alireza Tilkoo[1*], Seyed Mostafa Siadatmousavi[2], Barat Mojaradi[3]

[1,2,3] *University of Science and Technology of Iran, University St., Hengam St., Resalat Square, Tehran, Iran*

Abstract

Coastal environments are always under the pressure of natural processes such as erosion, sedimentation, natural disasters as well as human projects. These threats have made coastal areas a priority for coastline monitoring and sustainable coastal management programs. In this paper, algorithms for separating water and land boundaries as well as new sub-pixel methods are presented with the aim of dividing large pixels (with low resolution and spatial accuracy) into smaller pixels and creating a classified map with better spatial resolution. Different water identification indices and machine learning algorithms were investigated, and two models of Spatial Attraction Models were implemented. Results showed that the Sub-pixel / Sub-pixel Spatial Attraction Model had more capacity in providing higher resolution and precision, while provided 10% reduction in error when compared with observations. To skill assess these two methods, the difference in areas created by each method compared to the reference shoreline (high resolution aerial image) was computed. Also, in order to accurately evaluate and show the high accuracy of sub-pixel algorithms, the results of these algorithms should be examined by conventional classification methods. The creation of such models is proposed to support integrated coastal management in the Persian Gulf region for future studies.

© 2018 Published by INIOAS

Keywords: Subpixel algorithms, Shoreline, Spatial attraction model, Machine learning algorithms

1. Introduction

Coastal areas are critical and very complex environments; thus, various geophysical parameters must be continuously monitored. Nowadays, the use of spectral indices has gained more attention because they are considered as less restrictive and more reproducible methods, particularly for applications on a broad or global scales (Aires et al., 2017; Pekel, Cottam, Gorelick, & Belward, 2016). A variety of spectral indices have been developed recently to track surface water areas using satellite imagery (Jones, 2015; Lefebvre et al., 2019; McFeeters, 1996).

Due to the advances in remote sensing science and GIS, integrated techniques have been proposed to extract coastlines with different resolutions. In general, super resolution methods, first introduced by Atkinson in 1997(Atkinson, 1997), produce sub-pixel-level classification maps. Such algorithms are based on the spatial dependence within adjacent pixels (Sánchez-García, Balaguer-Beser, Almonacid-Caballer, & Pardo-Pascual, 2019; Xiong et al., 2018).

* Corresponding Author name: Alireza Tilkoo
E-mail address: alirezatilkoo@gmail.com

Downloaded from jpg.inio.ac.ir at 8:54 IRST on Sunday December 5th 2021

The nature of the real landscape and the process of obtaining information is complex because many mixed pixels exist in remote sensing images, which leads to difficulties in image inspection as well as its use (Nguyen, Atkinson, & Lewis, 2005). Assigning mixed pixels to a single class would result in loss of some information, which is not appropriate. Soft classifications estimate the proportion of each class within mixed pixels; these methods includes the fuzzy c-means classifier (Dewi & Bijker, 2019), decision tree (Poortinga et al., 2019), random forest (Zhou, Liu, & Zhang, 2019), and support vector machine (Elnabwy et al., 2020; Navale & Haldar, 2019).

Then, an integrated water body mapping method was introduced using satellite imagery HJ-1A/B. This method was invented based on a combination of the difference between NDVI [1] and NDWI using topographic slope and the near-infrared band (NIR). The NDVI-NDWI index is used to improve the contrast between water bodies and the surficial features around them. The topography slope is used to eliminate the shadow of the mountains, and the NIR band is used to remove the effects of terrestrial constructions (Lu et al., 2011). Liu et al. used the thresholding method on SAR[2] images for segmentation of these images. Their results included a detailed description of the geometric shape, the Antarctic coastlines features, and also, presenting a precise measure for future change detection studies (Liu and Jezek, 2004).

In order to improve the accuracy of the extraction of water in the presence of different sets of environmental noise, an index has been proposed, and at the same time, the threshold values for stability were proposed. The new Automated Water Extraction Index (AWEI) provides a high-precision classification for dark and shady areas, while, in these circumstances, other classification methods often encounter problems. The design of the AWEI index is based on the maximization of water and non-water pixel resolution through subtracting and adding up the bands, as well as the use of different coefficients. Finally, the two indices $AWEI_{nsh}$ and $AWEI_{sh}$ were presented. The AWEIch index is essentially formulated to improve the accuracy of the shadow pixels removal in urban areas, which cannot be remove by the $AWEI_{nsh}$ index, (Feyisa et al., 2014). Fisher et al. compared the water indices. Their results showed that the water index developed for various use in standard analyses of the upper atmospheric data (WI^{3}_{2006}), the new water index developed from separating linear analysis of surface reflection processing data (WI_{2015}) as well as the $AWEI_{sh}$ index with a total validation accuracy of 95-99%, for pure pixels and a total validation accuracy of 73-75% for mixed pixels, had better performance than other investigated indices (Fisher et al., 2016).

However, machine learning algorithms fail to identify the location of these classes in each pixel. Therefore, sub-pixel mapping or sub-pixel placement has been proposed as a way to remedy this problem (Wang, Zhang, Hao, & Wang, 2019).

These methods reduce the potential errors of spectral mixing. Generally Speaking, Spatial Attraction Models solve an inverse, illpossessed problem, because minimal image information is not sufficient to achieve the spatial distribution of groups on a subpixel scale (Song, Zhong, Ma, & Feng, 2019; Wang, Zhang, Zhang, et al., 2019). Spatial algorithms were introduced by creating functions between subpixels and pixels based on the theory of spatial dependence. In the SPSAM[4] model, attraction occurs between sub-pixels of the central pixel and eight adjacent pixels, but in the SSSAM[5] model, this occurs for sub-pixels and adjacent sub-pixels.(P. Wang & Wang, 2017; Q. Wang, Wang, & Liu, 2012). In this paper, the water spectral index and soft classifier were used along with

[1] NDVI
[2] Synthetic Aperture Radar
[3] Water Index
[4] Subpixel/Pixel Spatial Attraction Model
[5] Subpixel/Subpixel Spatial Attraction Model

Downloaded from jpg.inio.ac.ir at 8:54 IRST on Sunday December 5th 2021

spatial attraction models. A detailed description of spatial attraction algorithms is provided in Section 2.

2. Materials and Methods

The images used in this study are Landsat satellite images with a spatial resolution of 30 meters. Initially, the spatial resolution of images are increased to 15 meters using one of the methods of combining satellite images with the panchromatic band of Landsat multispectral images. Combining images at the pixel level is the most common level of image integration and is used to improve image quality for visual interpretation. GS* algorithm has been used to increase spatial resolution. Then, to reduce amount of the post calculations in MATLAB software processing, a smaller portion of the images were selected.

2.1. Integration of satellite images using GS algorithm

The images used in this study are obtained from the Landsat satellite images with a spatial resolution of 30 meters. First, by using one of the satellite image integration methods and the panchromatic band of Landsat multi-spectral images, the spatial resolution of the image is increased to 15 meters to exploit the data optimally. The most common level for integration of images is their integration at the pixel-level, and is used to improve the image quality for better visual interpretation. In this paper, the GS† algorithm has been used to increase the resolution of the Landsat images. The basis of this method is the use of the Gram-Schmidt orthogonalization, which consists of transforming a set of linearly independent vectors of a unitary space into a set of orthogonal vectors. The Gram–Schmidt process takes a finite, linearly independent set $S = \{u_1, u_2, ..., u_n\}$ and generates an orthogonal set $S' = \{v_1, v_2, ..., v_n\}$. The Gram–Schmidt process then works as follows:

Step 1: $v_1 = u_1$ (1)

Step 2: $v_2 = u_2 - \mathrm{Proj}_{v_1}(u_2)$ (2)

Step 3: $v_3 = u_3 - \mathrm{Proj}_{v_1}(u_3) - \mathrm{Proj}_{v_2}(u_3)$ (3)

Step n: $v_n = u_n - \sum_{j=1}^{n-1} \mathrm{Proj}_{v_j}(u_n)$ (4)

Where Proj_v is the projection map. By averaging the multispectral image bands, the GS algorithm creates a simulated panchromatic band. In the following, GS transformation is presented on multi-spectral image bands and simulated panchromatic bands.

2.2. SVM classification

In this section, water spectral indices as well as the SVM classification method are used to distinguish between water and land boundaries. The Support Vector Machine method is based on statistical learning theory, which was first used in 1960, and it is a supervised nonparametric statistical method (Rokni et al., 2015). In SVM method,

* Gram-Schmidt spectral sharpening
† Gram-Schmidt

Downloaded from jpg.inio.ac.ir at 8:54 IRST on Sunday December 5th 2021

boundary cases are called support vectors, and to calculate the decision-making boundary of two completely separated classes, the optimal margin method is used. This optimal margin is calculated in such a way that all samples of the two classes are located on both sides of the boundary, and the optimal boundary is the boundary with the greatest distance between the samples of the two classes (Pao, 1989).

Based on structural risk minimization, the problem of optimization is solved, and its goal is to maximize the margins between the optimal hyperplane separator and the closest training samples called support vectors. The final hyperplane decision function can be defined as:

$$f(x) = \sum_{i=1}^{L} \alpha_i y_i k(x_i, x_j) + \gamma \tag{5}$$

where α_i are Lagrange multipliers and $k(x_i, x_j)$ is a kernel function. A general description of the concept of SVM method is given in detail in these resources (Burges, 1998). In this paper, the proposed method utilized RBF kernel

$$k(x, x') = \exp(-\lambda \|x - x'\|^2) \tag{6}$$

Implementing a kernel-based SVM involves the selection of multiple parameters, as well as kernel parameters and regularization parameters. Exploring a grid is a known method for choosing a model that performs a search and generates the best fit for parameter values. The proposed strategy applies grid search as the model selection of SVM classifier. The search range for *C* is $[2^{-2}, 2^{10}]$, and $[2^{-10}, 2^{2}]$ for γ in RBF kernel.

The Modified Normalized Difference Water Index (MNDWI) spectral index was used to extract coastlines. Land cover ratios must be determined by one of the soft classification methods. The support vector machine (SVM) classification method was employed which is a supervised learning system based on recent advancements in statistical learning theory. SVM was developed for binary classification. A number of studies have focused on the mathematical relationships for SVMs.

It requires a dataset for training phase. In this study, according to the purpose of extracting the coastline, the selection of two training areas (ROI) is sufficient. Spatial attraction algorithms are applied to these areas. In the following, each of these two algorithms is presented briefly.

2.3. SPSAM Classification

In a subpixel/ spatial attraction model (SPSAM), the attraction between each subpixel in pixels of coarse resolution and its neighboring pixels is calculated to determine the subpixel spatial distribution of each class (Q. Wang et al., 2012). Assumptions of this approach is as follows: the model acts on the basis of fraction values in neighboring pixels relative to subpixels in a central pixel. A subpixel can only be attractted by pixels around the center pixel (which includes the subpixel); as a result, the maximum of eight neighboring pixels can be considered for attraction, and the rest of pixels are too far to be attracted (Mertens, De Baets, Verbeke, & De Wulf, 2006). The formulas of this method are:

$$SD_{cf} = \sum_{k=1}^{N_A} \omega_k F_c(P_k) \tag{7}$$

Downloaded from jpg.inio.ac.ir at 8:54 IRST on Sunday December 5th 2021

$$D_{c\cdot ij} = \sum_{k=1}^{N_A} \omega_k F_c(P_k) = \sum_{k=1}^{N_A} \frac{F_c(P_k)}{d_k} \quad (8)$$

where $\mathbf{SD_{cf}}$ is the measure of spatial dependence of class c to subpixel $\mathbf{pf}$, $\mathbf{N_A}$ is the number of neighboring pixels, $\boldsymbol{\omega_k}$ is the weight of spatial dependence, $\mathbf{F_c(P_k)}$ is the proportion of the kth neighbor pixel $\mathbf{P_k}$ to class c, and $\mathbf{d_k}$ is the Euclidean distance between geometric centers of subpixel $\mathbf{p_{ij}}$ and its neighbor pixel $\mathbf{P_k}$.

2.4. SSSAM Classification

In the SPSAM method, the subpixels of each neighbor of the central pixel were considered to be the central points of the neighboring pixel. Then the spatial attraction for the class c is calculated for the subpixel $\mathbf{p_{ij}}$ from each neighboring pixel as the attractor between the $\mathbf{p_{ij}}$ center and its neighbor center. Clearly, this description of attraction is not always correct because the subpixels of the internal pixel may not be entirely close to the central point. Instead, they may be located at a corner or near to a boundary of that pixel so that each pixel cannot be considered as a point (Q. Wang et al., 2012). In SSSAM method, the spatial attraction of each neighboring pixel is the sum of the attraction between the center $\mathbf{p_{ij}}$ and the center of each subpixel in the neighboring pixel. Suppose $\mathbf{p_m}$ is a subpixel within $\mathbf{P_k}$, and $\mathbf{d_m}$ is the Euclidean distance between geometric centers of subpixels $\mathbf{p_{ij}}$ and $\mathbf{p_m}$; then the $\mathbf{SD_{cf}}$ can be calculated as (L. Wang, Wang, & Liu, 2011) :

$$SD_{cf} = \sum_{k=1}^{N_A} \omega_k F_c(P_k) = \sum_{k=1}^{N_A} \omega_k \frac{F_c(P_k) S^2}{S^2} = \frac{1}{S^2} \sum_{m=1}^{N_A S^2} \omega_k x_{cm} = \frac{1}{S^2} \sum_{m=1}^{N_A S^2} \frac{x_{cm}}{d_m} \quad (9)$$

Mixed pixel $\mathbf{P_{ab}}$ in the coarse low resolution image (i.e. fraction image) is selected. Attractions for subpixels within $\mathbf{P_{ab}}$ caused by each class from neighbors are calculated according to equation (3). The subpixels with the highest attraction values are allocated to the corresponding class. The flowchart of the research process is given in Figure 1.

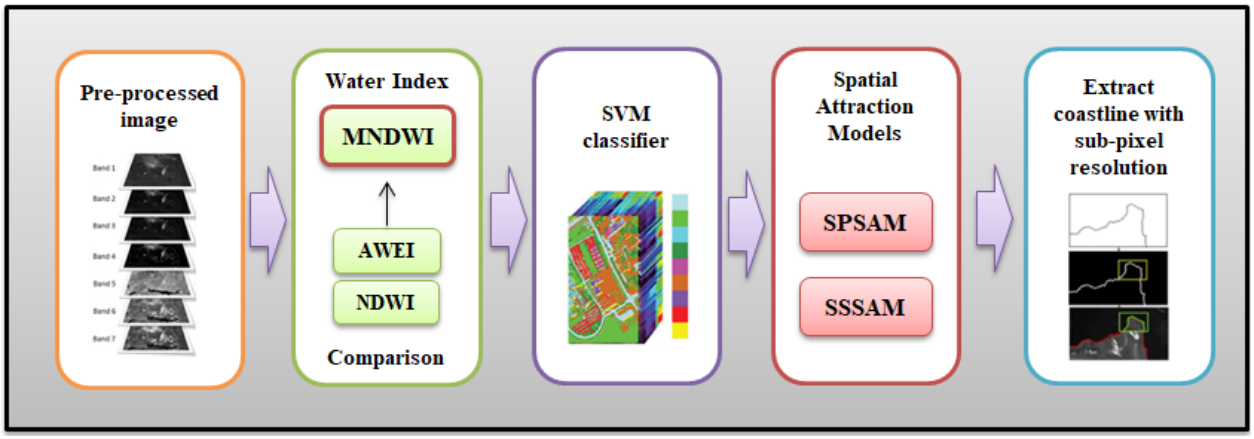

Fig. 1: Flowchart of the proposed methodology for extraction coastlines

Downloaded from jpg.inio.ac.ir at 8:54 IRST on Sunday December 5th 2021

3. Results

In this research, three spatial subsets have been cut from Landsat satellite imagery from rocky areas of Hormozgan province close to Bonod and Tobon coasts. It should be noted that the choice of rocky parts of the coastal areas has been made to ignore tidal changes. To evaluate the accuracy of the methods in extracting the coastline, the difference between the areas created between the estimated coastline from each method and the reference coastline should be calculated. It is important to note that the drawing lines on the raster vector are hard to classify without smoothing, and the reference shoreline is drawn using aerial images with a pixel accuracy of 20 cm. It is clear that the method, which provides a smaller total area, has better accuracy in extracting coastlines. Due to the limited number of pages of the article, the results of one area are displayed (area 2). Figure 2 shows the three parts of area 2 with reference lines (aerial photographs) and the estimated coastline from each method.

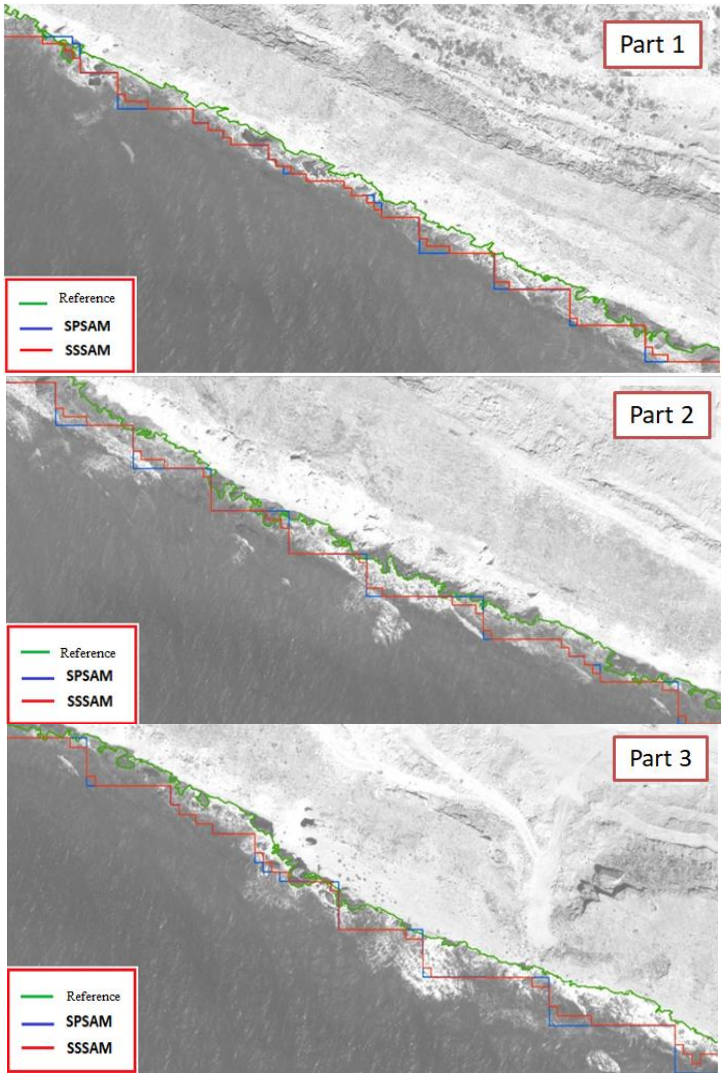

Fig. 2: There are 3 parts of area 2 with a rocky part and close to the coasts of Bonoud. The colors are green, blue, and red, respectively, for the shoreline, the reference extracted from the aerial image, and the output of the SPSAM and SSSAM methods.

Downloaded from jpg.inio.ac.ir at 8:54 IRST on Sunday December 5th 2021

4. Discussion and conclusion

According to the error index for 3 study areas, the SSSAM method outperformed SPSAM method. The SPSAM method makes more mistakes due to the fact that it considers only the central values of the adjacent pixels and ignores the values of the corners. In contrast, in SSSAM method, these values are considered. The total area difference of the SSSAM method is less than the SPSAM method (Table 1). From the ratio of the obtained areas, the reduction of the error of the second method can be estimated as ~10%.

It should be noted that better results occurred when appropriate water spectral index and better classifier were used. In the latest research on the extraction of water bodies and between types of spectral indices, the combination of SVM classification with MNDWI index has achieved the best results among related techniques with desirable spatial and spectral quality. For this reason, this technique was used in this study. Table 2 shows the comparison between the Support Vector Machine (SVM) with the results of two sub-pixel algorithms on area 3.

Table 1: Differences in areas for each method and the reference shoreline (area 2)

Methods	Total areas (m^2)
SPSAM	5577.29
SSSAM	5189.57

Table 2: Comparison between methods on area 3

Methods	Total areas (m^2)
SPSAM	3386.29
SSSAM	3593.67
Support Vector Machine	4471.62

References

Aires, F., Miolane, L., Prigent, C., Pham, B., Fluet-Chouinard, E., Lehner, B., & Papa, F. (2017). A global dynamic long-term inundation extent dataset at high spatial resolution derived through downscaling of satellite observations. *Journal of Hydrometeorology*, *18*(5), 1305-1325.

Atkinson, P. M. (1997). Mapping sub-pixel boundaries from remotely sensed images. *Innovations in GIS, 4*, 166-180.

BURGES, C. J. 1998. A tutorial on support vector machines for pattern recognition. *Data mining and knowledge discovery,* 2**,** 121-167.

Dewi, R. S., & Bijker, W. (2019). Dynamics of shoreline changes in the coastal region of Sayung, Indonesia. *The Egyptian Journal of Remote Sensing and Space Science*.

Elnabwy, M. T., Elbeltagi, E., El Banna, M. M., Elshikh, M. M., Motawa, I., & Kaloop, M. R. (2020). An Approach Based on Landsat Images for Shoreline Monitoring to Support Integrated Coastal Management—A Case Study, Ezbet Elborg, Nile Delta, Egypt. *ISPRS International Journal of Geo-Information*, *9*(4), 199.

FEYISA, G. L., MEILBY, H., FENSHOLT, R. & PROUD, S. R. 2014. Automated Water Extraction Index: A new technique for surface water mapping using Landsat imagery. *Remote Sensing of Environment,* 140**,** 23-35.

Downloaded from jpg.inio.ac.ir at 8:54 IRST on Sunday December 5th 2021

FISHER, A., FLOOD, N. & DANAHER, T. 2016. Comparing Landsat water index methods for automated water classification in eastern Australia. *Remote Sensing of Environment*, 175**,** 167-182.

Jones, J. W. (2015). Efficient wetland surface water detection and monitoring via landsat: Comparison with in situ data from the everglades depth estimation network. *Remote sensing*, *7*(9), 12503-12538.

Lefebvre, G., Davranche, A., Willm, L., Campagna, J., Redmond, L., Merle, C.,... Poulin, B. (2019). Introducing WIW for detecting the presence of Water In Wetlands with Landsat and Sentinel satellites. *Remote sensing*, *11*(19), 2210.

LIU, H. & JEZEK, K. 2004. Automated extraction of coastline from satellite imagery by integrating Canny edge detection and locally adaptive thresholding methods. *International journal of remote sensing*, 25**,** 937-958.

LU, S., WU, B., YAN, N. & WANG, H. 2011. Water body mapping method with HJ-1A/B satellite imagery. *International Journal of Applied Earth Observation and Geoinformation*, 13**,** 428-434.

McFeeters, S. K. (1996). The use of the Normalized Difference Water Index (NDWI) in the delineation of open water features. *International Journal of Remote Sensing*, *17*(7), 1425-1432.

Mertens, K. C., De Baets, B., Verbeke, L. P., & De Wulf, R. R. (2006). A sub- pixel mapping algorithm based on sub-pixel/pixel spatial attraction models. *International Journal of Remote Sensing*, *27*(15), 3293-3310.

Navale, A., & Haldar, D. (2019). Evaluation of machine learning algorithms to Sentinel SAR data. *Spatial Information Research*, 1-11.

Nguyen, M. Q., Atkinson, P. M., & Lewis, H. G. (2005). Superresolution mapping using a Hopfield neural network with LIDAR data. *IEEE Geoscience and Remote Sensing Letters*, *2*(3), 366-370.

Pekel, J.-F., Cottam, A., Gorelick, N., & Belward, A. S. (2016). High-resolution mapping of global surface water and its long-term changes. *Nature*, *540*(7633), 418-422.

Poortinga, A., Tenneson, K., Shapiro, A., Nquyen, Q., San Aung, K., Chishtie, F., & Saah, D. (2019). Mapping plantations in Myanmar by fusing landsat-8, sentinel-2 and sentinel-1 data along with systematic error quantification. *Remote sensing*, *11*(7), 831.

PAO, Y. 1989. Adaptive pattern recognition and neural networks.

ROKNI, K., AHMAD, A., SOLAIMANI, K. & HAZINI, S. 2015. A new approach for surface water change detection: Integration of pixel level image fusion and image classification techniques. *International Journal of Applied Earth Observation and Geoinformation*, 34**,** 226-234.

Sánchez-García, E., Balaguer-Beser, Á., Almonacid-Caballer, J., & Pardo-Pascual, J. E. (2019). A new adaptive image interpolation method to define the shoreline at sub-pixel level. *Remote sensing*, *11*(16), 1880.

Song, M., Zhong, Y., Ma, A., & Feng, R. (2019). Multiobjective sparse subpixel mapping for remote sensing imagery. *IEEE Transactions on Geoscience and Remote Sensing*, *57*(7), 4490-4508.

Wang, L., Wang, Q., & Liu, D. (2011). *Sub-pixel mapping based on sub-pixel to sub-pixel spatial attraction model.* Paper presented at the Geoscience and Remote Sensing Symposium (IGARSS), 2011 IEEE International.

Wang, P., & Wang, L. (2017). Soft-then-hard super-resolution mapping based on a spatial attraction model with multiscale sub-pixel shifted images. *International Journal of Remote Sensing*, *38*(15), 4303-4326.

Wang, P., Zhang, G., Hao, S., & Wang, L. (2019). Improving remote sensing image super-resolution mapping based on the spatial attraction model by utilizing the pansharpening technique. *Remote sensing*, *11*(3), 247.

Wang, P., Zhang, L., Zhang, G., Bi, H., Dalla Mura, M., & Chanussot, J. (2019). Superresolution land cover mapping based on pixel-, subpixel-, and superpixel-scale spatial dependence with pansharpening technique. *IEEE Journal of Selected Topics in Applied Earth Observations and Remote Sensing*, *12*(10), 4082-4098.

Wang, Q., Wang, L., & Liu, D. (2012). Integration of spatial attractions between and within pixels for sub-pixel mapping. *Journal of Systems Engineering and Electronics*, *23*(2), 293-303.

Xiong, L., Deng, R., Li, J., Liu, X., Qin, Y., Liang, Y., & Liu, Y. (2018). Subpixel surface water extraction (SSWE) using Landsat 8 OLI data. *Water*, *10*(5), 653.

Zhou, X., Liu, X., & Zhang, Z. (2019). *Automatic Extraction of Lakes on the Qinghai-Tibet Plateau from Sentinel-1 SAR Images.* Paper presented at the 2019 SAR in Big Data Era (BIGSARDATA).

Downloaded from jpg.inio.ac.ir at 8:54 IRST on Sunday December 5th 2021